15. MINOR PLANETS AND PLANETARY SATELLITES

Some 48 minor planets and three natural satellites were observed during the Hipparcos main mission with the purpose of linking the dynamical and kinematical reference systems and for dynamical and physical studies of these solar system bodies. This chapter describes specific aspects of the processing implemented for the solar system objects in order to derive the astrometric and photometric solutions. Several summary tables related to the minor planets and their observability conditions are also included in this chapter.

15.1. Introduction

The observation of minor planets and natural satellites of giant planets with Hipparcos was considered during the mission planning to be of high scientific relevance with the goal of obtaining accurate astrometric positions and investigating the relationship between the dynamical and kinematical reference systems. Some 60 minor planets were included in the preliminary program, of which 48 were repeatedly observed during the actual mission together with three planetary satellites (J II Europa, S VI Titan and S VIII Iapetus) yielding astrometric and photometric data of excellent quality. The corresponding star mapper observations are described in Volume 4, Chapter 15.

As a result of the rapid and non-linear motion of these objects over a time-span of only a few hours, the basic data treatment had to be adapted for these objects to produces one-dimensional astrometric positions on the reference great circles on which they were observed. The solar system objects were observed in the same way as stellar objects. However objects with an apparent diameter larger than 0.05 arcsec were resolved by the Hipparcos telescope and the astrometric solution refers more or less to the photocentre of the illuminated fraction of the disc, i.e. to a point varying with the phase angle. In the first section of this chapter the main properties of the grid signal pertaining to the minor planets are emphasised. Then the astrometric solution on the great circle is presented, followed by the photometric aspects of the processing.

15.2. Hipparcos Observations of an Extended Source

The signal recorded behind the Hipparcos main grid during the transit of a light source was modelled by the ‘five-parameter model’ introduced in Chapter 5. It was shown that

the periodic signal for a point-like source could be accurately represented by a Fourier series up to the second harmonic as:

$$S(t) = I_0\,[1 + M_0\cos(\omega t + \phi_0) + N_0\cos 2(\omega t + \phi_0)] \qquad [15.1]$$

where M_0, N_0 are the calibrated modulation coefficients, and ϕ_0 is the modulation phase of the signal, corresponding to the position of the source on the grid at the reference time $t = 0$. ω is the time frequency of the signal. For an object of significant angular size, typically with a diameter $\rho \gtrsim 0.05$ arcsec, the modulated signal results from the integration of the point-like signal over the surface of the source. This gives a signal of the same form (Morando 1986, Lindegren 1986, Morando & Lindegren 1989):

$$S(t) = I\ [1 + M\cos(\omega t + \phi) + N\cos 2(\omega t + \psi)] \qquad [15.2]$$

but now with reduced modulation coefficients M, N and (in general) shifted modulation phases ϕ, ψ depending on the brightness distribution of the apparent disc. Let $x = \pi\rho/s$ be a dimensionless variable relating the angular diameter of the planet to the grid period, $s = 1.2074$ arcsec. Introduce the complex function:

$$U(x) = \iint I_\sigma \exp(-\imath x\mathbf{w}'\mathbf{n})\mu\,\mathrm{d}\sigma$$

where I_σ is the specific brightness of the surface element $\mathrm{d}\sigma$, $\imath = \sqrt{-1}$, $\mathbf{w}$ the unit vector in the scanning direction (Figure 15.6), $\mathbf{n}$ the unit vector normal to the surface element, and μ the cosine of the angle of reflection. The total intensity and the degradation of the modulation coefficients can then be written:

$$I = U(0), \qquad \frac{M}{M_0} = \left|\frac{U(x)}{U(0)}\right|, \qquad \frac{N}{N_0} = \left|\frac{U(2x)}{U(0)}\right| \qquad [15.3]$$

and the phase shifts are:

$$\phi - \phi_0 = \arg[U(x)], \qquad \psi - \psi_0 = \tfrac{1}{2}\arg[U(2x)] \qquad [15.4]$$

In interferometric terminology, $U(nx)/U(0)$ is the complex visibility of the object, in the direction of $\mathbf{w}$, at n times the spatial frequency of the grid.

The abscissa was derived from the phase ϕ of the first harmonic in NDAC, and by means of a weighted average of the two phases, $0.75\phi + 0.25\psi$, in FAST. The major consequences for an extended object are that (i) the observed position does not strictly correspond to the definition of the photocentre, and (ii) the FAST and NDAC observed positions do not strictly correspond to the same point. Introducing the functions:

$$\begin{aligned} j_1(x,\,\alpha) &= J_1(x) + J_1(x\cos\alpha) \\ h_1(x,\,\alpha) &= \boldsymbol{H}_1(x) - \boldsymbol{H}_1(x\cos\alpha) \end{aligned} \qquad [15.5]$$

where α is the solar phase angle, and J_1, $\boldsymbol{H_1}$ are the Bessel and Struve functions respectively, then for a uniformly bright sphere and a scan along the intensity equator:

$$U(x) = j_1(x,\,\alpha) + \imath h_1(x,\,\alpha) \qquad [15.6]$$

which yields the phase offset relative to the centre of figure. The difference between the photocentre and the position assigned from the phases, using the FAST and NDAC procedures, is shown in Figure 15.1 as a function of the apparent diameter of the planet. For a phase angle of $\alpha = 20°$, typical for the Hipparcos observations of minor planets

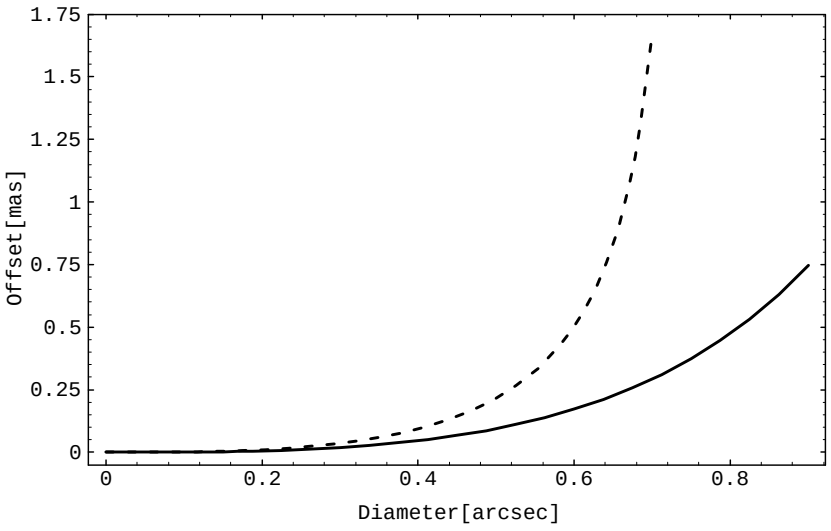

Figure 15.1. *Theoretical difference between the observed position and the photocentre versus apparent diameter. The curves are for a spherical object of uniform brightness viewed with a solar phase angle $\alpha = 20°$. Solid curve: positions derived from the first harmonic only (NDAC). Dashed curve: positions derived from a weighted mean of the harmonics (FAST) — this method is practically limited to objects smaller than 0.7 arcsec.*

(Figure 15.10), the differences remain well below one milliarcsec except for (1) Ceres as observed by FAST at its maximum diameter, $\rho \sim 0.7$ arcsec.

The Hipparcos magnitude of the minor planets was estimated in the same way as for the stars and is described in Chapter 14. The magnitude $Hp_{\rm dc}$ was directly derived from the mean intensity I of the signal (corrected for sky background), while $Hp_{\rm ac}$ was based on the amplitudes IM and IN of the modulated components of the signal. Then from Chapter 14:

$$\Delta Hp \equiv Hp_{\rm ac} - Hp_{\rm dc} \simeq -2.5 \log_{10} \frac{M M_0 + N N_0}{M_0^2 + N_0^2} \qquad [15.7]$$

$Hp_{\rm ac}$ is a biased estimator for the larger planets, depending on the apparent diameter at the time of observation, through the attenuation of the modulation measured by M/M_0 and N/N_0.

In the approximation of a spherical object of uniform brightness at zero solar phase angle, the imaginary part of $U(x)$ vanishes because of the azimuthal symmetry of the problem. Therefore $U(x)$ is simply given by the Hankel transform of order zero:

$$\mathcal{H}_0[1;\, x] = \int_0^1 J_0(xr) r \, {\rm d}r \qquad [15.8]$$

and the attenuation in the modulation coefficients can be expressed as a function of the apparent size of the source:

$$\frac{M}{M_0} = 2\,\frac{|J_1(x)|}{x}, \qquad \frac{N}{N_0} = \frac{|J_1(2x)|}{x} \qquad [15.9]$$

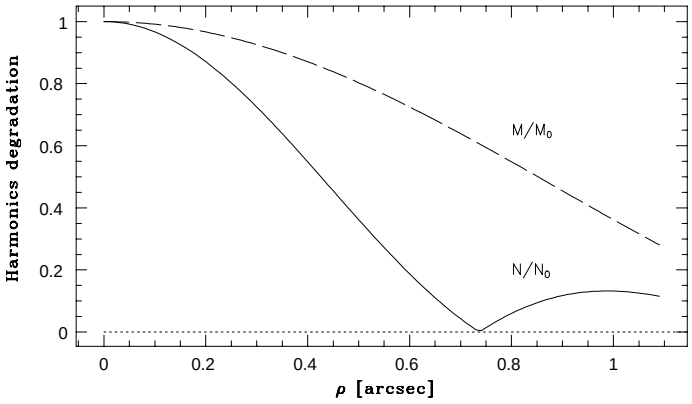

Figure 15.2. *Attenuation of the modulation coefficients for the first (dashed line) and second harmonics (solid line) for a spherical object of uniform brightness and of apparent diameter ρ.*

These functions are plotted in Figure 15.2. There is no significant attenuation in the signal modulation up to an apparent diameter of about 0.1 arcsec for the first harmonic and 0.05 arcsec for the second harmonic.

15.3. Astrometry on the Circle

Transformation to Astrometric Directions

In the great-circle reduction a one-dimensional position was obtained, about twice per day, for the Hipparcos stars observed in that interval. This great-circle abscissa was calculated by fitting all the grid coordinates of a star collected during the great-circle interval of several hours. The main principles of this process, outlined in Chapter 9, apply also to the observations of the solar system objects. However, because of the rapid and non-linear motion of the planets, a different sampling time was adopted for these objects, leading to one great-circle abscissa for every observational frame of 32/15 s. For the final catalogue, normal positions were derived at a rate of one astrometric one-dimensional position per field–transit of the object across the instrument main grid.

The instantaneous Hipparcos observations referred to the proper direction of the planet; thus the first step of the processing consisted of transforming this direction into the coordinate direction by computing the stellar component of the aberration and the parallax introduced by the satellite's motion around the Earth. These corrections were evaluated to an accuracy better than one milliarcsec, which required the modelling of the aberration to the second order in $|\mathbf{V}|c^{-1}$, where $\mathbf{V}$ is the barycentric velocity of Hipparcos. Likewise, the light bending by the spherical potential of the Sun was taken into account to first order in $GS/ac^2 \simeq 2$ mas where a, the heliocentric distance of the satellite, is close to $A \simeq 1$ AU (see Table 12.1). The deflection by the giant planets was neglected.

Most minor planets have a sizeable apparent diameter (> 0.05 arcsec) compared to the Hipparcos astrometric accuracy, and the solar phase angle effect shifts the photocentre

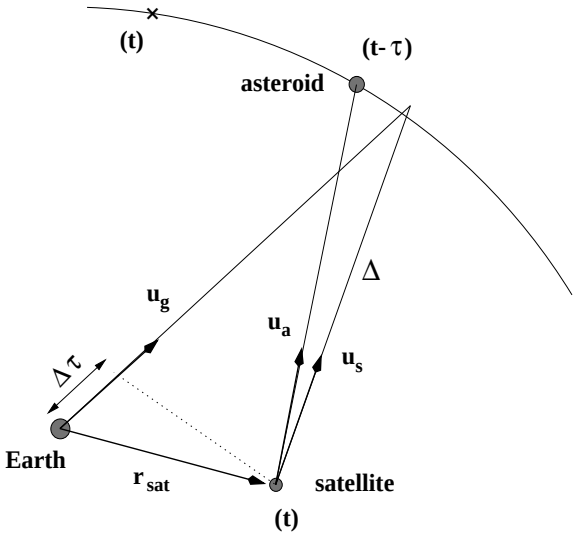

Figure 15.3. *Coordinate direction of a minor planet. The observed satellitocentric proper direction* $\mathbf{u}_a$ *is first corrected for stellar aberration and light deflection into* $\mathbf{u}_s$*. It is then transformed into the (geocentric) coordinate direction* $\mathbf{u}_g$*. The epoch of observation at the satellite is also corrected by* $\Delta\tau$ *into an epoch at the geocentre.*

with respect to the centre of figure. As this cannot be evaluated within the required accuracy without a rather sophisticated and uncertain modelling of the light diffusion on the surface, no phase correction was applied and the direction provided by Hipparcos corresponds in the first approximation to the position on the sky of the instantaneous photocentre (see Section 15.2).

Let $\mathbf{u}_a$ be the apparent (or 'proper') satellitocentric direction of a solar system object, and $\mathbf{u}_g$ its geocentric astrometric (or 'coordinate') direction, with $|\mathbf{u}_a| = |\mathbf{u}_g| = 1$ (see Figure 15.3 and Chapter 12). These vectors are referred to a coordinate frame associated with a given reference great circle, the so-called reference great-circle frame (Section 11.2). The one observed quantity was the apparent abscissa (v) on the reference great circle, while the perpendicular coordinate (r) was computed from the ephemerides. The initial conditions for the ephemerides of minor planets were taken from the ' Ephemerides of minor planets for the year 1992' and were numerically integrated with a Bulirsch-Stoer integrator including the perturbations of all the major planets from Mercury to Neptune. The planetary positions were taken from the JPL solar system ephemerides DE200.

The direction $\mathbf{u}_a$ was first transformed into a satellitocentric astrometric direction, $\mathbf{u}_s$, by correcting for the aberration and gravitational light bending. This was actually done as part of the same processing as applied to the stars, namely in the great-circle reductions (Chapter 9). The satellitocentric astrometric direction was then transformed into the geocentric astrometric direction, $\mathbf{u}_g$, by applying the parallactic correction. The relationship between the apparent direction and the direction corrected for stellar aberration (the 'natural' direction) is given by inverting Equation 12.7 to the second order in V/c:

$$\hat{\mathbf{u}}_s = \left\langle \mathbf{u}_a - \left[1 - \frac{\mathbf{V}'\mathbf{u}_a}{2c}\right]\frac{\mathbf{V}}{c}\right\rangle + O\left(\frac{|\mathbf{V}|}{c}\right)^3 \qquad [15.10]$$

where $\mathbf{V}$ is the barycentric velocity of the Hipparcos satellite. The barycentric velocity of the Earth was provided by a compact representation of the ephemeris BDL 82 (see

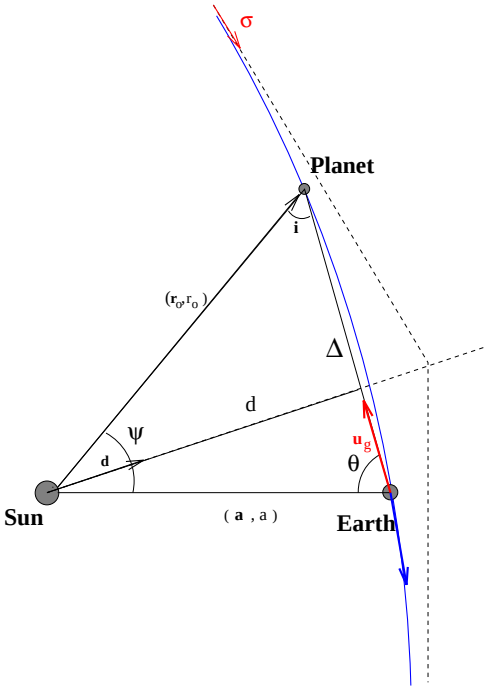

Figure 15.4. *Notations for the correction of gravitational light deflection.*

Chapter 12 and Chapront *et al.* 1984), while the geocentric velocity of the spacecraft was provided by the mission operations centre, ESOC. The velocity vector **V** was computed as the sum of these two velocities after transformation to the same reference system.

The application of the gravitational light deflection for a source at finite distance from the Sun leads to the following expression for the astrometric direction ($\mathbf{u}_s$) in terms of the natural direction ($\hat{\mathbf{u}}_s$):

$$\mathbf{u}_s = \left\langle \mathbf{u}_a - \mathbf{d}\,\frac{2GS}{a\,c^2}\,\tan\frac{\Psi}{2} \right\rangle + O\left(\frac{GS}{a\,c^2}\right)^2 \qquad [15.11]$$

with $\mathbf{d} = \langle \mathbf{u}_s \times (\mathbf{r}_0 \times \mathbf{u}_s) \rangle$ the unit vector along the impact radius, GS the heliocentric gravitational constant and c the speed of light (see Table 12.1); a is the heliocentric distance of the satellite (i.e. $a \simeq A$), and Ψ the heliocentric angle between the object and the satellite (see also Figure 15.4 for notations).

After these two steps $\mathbf{u}_s$ must be transformed into the geocentric direction $\mathbf{u}_g$, which gives:

$$\mathbf{u}_g = \langle \mathbf{u}_s \Delta + \mathbf{r}_{sat} \rangle \qquad [15.12]$$

where the geocentric position of Hipparcos, $\mathbf{r}_{sat}$, was provided with an accuracy of $\simeq$ 2 km by the satellite orbit determination performed at ESOC. Δ is the distance between Hipparcos and the minor planet, which for this correction had to be known to $\simeq$ 15 000 km, a requirement easily satisfied by the available ephemerides. The epoch of observation was also corrected for the first order light-time difference due to the geocentric orbit, $\Delta\tau = (g - \Delta)/c$, yielding the time at the geocentre, where $g = |\mathbf{u}_s \Delta + \mathbf{r}_{sat}|$ is the geocentric distance to the planet (see Figure 15.3).

Construction of a Normal Place in NDAC

A normal place was derived for every field–transit from the $\simeq 8$ consecutive abscissae measured at the frame level. In NDAC, the normal place was constructed from a fit of the observed abscissae to the linear motion of a planet in the time interval of a field crossing, about 19 s. In the first stage of the great-circle reduction, all the data were stored and a temporary file was created for every object observed on the circle. This file contained a reference time t_R, a reference abscissa v_R, the rate $q = dv/dt$, and a mean ordinate r_R for each object. For a solar system object, the ephemeris was used to compute a predicted abscissa and ordinate for the first and last frame of the transit (v_1, r_1 and v_n, r_n) corresponding to the mid-frame times (t_1, t_n). With the reference abscissa $v_R = (v_1+v_n)/2$, the reference time $t_R = (t_1+t_n)/2$, the abscissa rate $q = (v_n - v_1)/(t_n - t_1)$, and the mean ordinate $r_R = (r_1 + r_n)/2$, the residual of the abscissa in the kth frame, at time t_k, was:

$$\delta v_k = v_k - G\left(v_R + (t_k - t_R)q,\, r_R\right) \qquad [15.13]$$

where $G(v, r)$ is the transformation to grid coordinate, including attitude and instrument modelling. The result of the great-circle reduction was a weighted mean correction $\overline{\delta v}$ to the reference abscissa, so that the output for each transit consisted of t_R, $v_R + \overline{\delta v}$ and r_R. Transits were discarded when the signal was too faint to be useful, or in the case of a pointing offset exceeding 10 arcsec, making the reliability of the data questionable.

The results thus obtained in the final NDAC great-circle reductions were further corrected for the abscissa zero point errors determined in the corresponding sphere solution (N37.5; see Chapter 16). They were then transformed from the reference frame of N37.5 to the provisional system H37C realised by the merging of the final FAST and NDAC sphere solutions (see Chapter 17). This transformation was slightly different from, but practically equivalent to, the subsequent transformation to ICRS described in Section 15.4. It was applied as a correction to the abscissa:

$$v_{H37C} = v_{N37.5} - \boldsymbol{\varepsilon}'\mathbf{R} \qquad [15.14]$$

where $\mathbf{R}$ denotes the (positive) pole of the reference great circle, and $\boldsymbol{\varepsilon}$ is the time-dependent rotation detailed in Table 15.1.

Construction of a Normal Place in FAST

Unlike NDAC the normal place in FAST was based on the median of the abscissae. A typical situation of the abscissae at the frame level used to construct the normal place is shown in Figure 15.5. After the reduction on the sphere, a dedicated file was constructed for all the solar system objects to store the abscissae at each mid-frame time. The corrections to the origins δv_0 (Chapter 16) were available separately and used to obtain the abscissae in a consistent reference frame.

Let v_R be the reference abscissa at mid-transit time and $q = dv/dt$ based on the planet ephemeris. The observation equation for the reference abscissa was then: $v_R = v_k - (t_k - t_R)q$. The resulting reference abscissa was eventually estimated as the median $\bar{v}$ of the $n \simeq 8$ values $v_k - (t_k - t_R)q$ in a transit. The output for each transit consisted of t_R, $\bar{v} + \delta v_0$, r_R and the standard error of the reference abscissa, given by:

$$\sigma_v^2 = \frac{\pi}{2n}\,\frac{1}{n-1}\sum_k \left(\frac{\sigma_0}{\sigma_k}\,\eta_k\right)^2 = \frac{\pi}{2n}\,\tilde{\sigma}_0^2 \qquad [15.15]$$

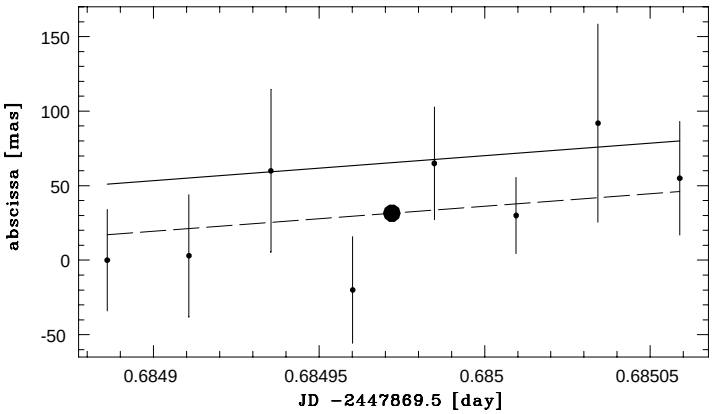

Figure 15.5. *Reduction of the minor planets abscissae at the transit level. A normal place for each transit was constructed by fitting the location parameter of a linear motion whose speed was taken from the ephemeris (solid line). The normal position (circle) corresponds to an average position of the frame level positions (mean in NDAC, median in FAST). The great-circle abscissa origin on the plot is arbitrary.*

where $\eta_k = v_k - v_R - (t_k - t_R)q$ are the residuals, and $\sigma_0 \eta_k / \sigma_k$ the weighted residuals. $\tilde{\sigma}_0^2$ is an estimator of the variance of a single observation. Usually there were $n = 8$ observations per transit.

Dubious abscissae v_k with an uncertainty greater than 150 mas were systematically discarded. In order to identify transits possibly corrupted by the presence of a parasitic star in the complementary field of view, observations with $\sigma_{\Delta Hp} > 0.3$ mag were rejected, where ΔHp is the difference between the ac- and dc-magnitudes (see Equation 15.7). Two other tests were constructed to filter out unreliable transits. Transits with estimated $\tilde{\sigma}_0 > 2\sigma_0$, or containing only one frame, were rejected. Likewise, a transit was rejected if it led to a magnitude difference between the ac- and dc-scales such that:

$$|\Delta Hp - \Delta Hp_{\rm calc}| > 5\sigma_{\Delta Hp} \qquad [15.16]$$

with $\Delta Hp_{\rm calc} \simeq 1.214\rho^2 + 0.03\rho^4$ derived from Equations 15.7 and 15.9 for an object of uniform brightness of apparent diameter ρ. The reference time was taken as the mean of the first and last used frame of a transit. The resulting positions were in the reference frame of the final FAST sphere solution, F37.3.

15.4. Astrometry Final Output

Transformation to the Tangent Plane

Each observation of a solar system object is uniquely defined by the time, the abscissa and the orientation of the circle on which the planet position was projected. It was, however, considered that a different presentation of the results would be more convenient for the users, although it was not possible to provide strictly two-dimensional positions. The Hipparcos observations of solar system objects are supplied as an observation equation relating the abscissa to a perfectly defined reference point (α_0, δ_0) (see

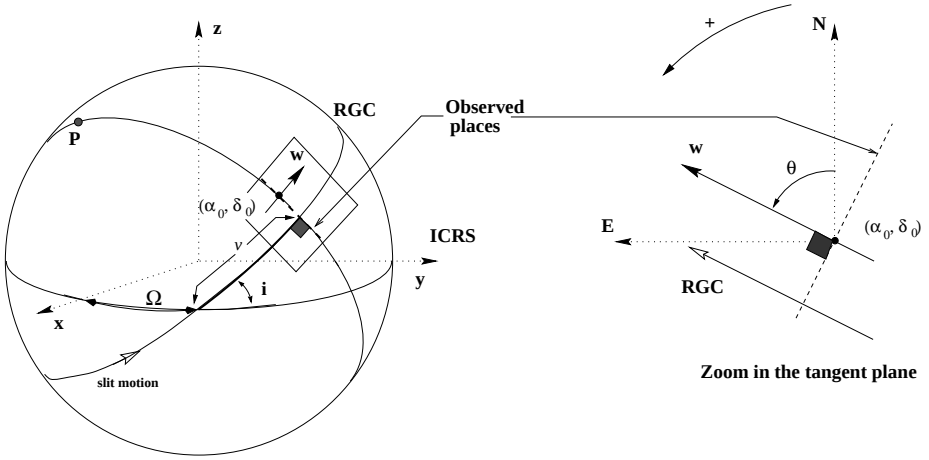

Figure 15.6. *Transformation to the tangent plane. See text for details.*

Figure 15.6). More precisely, the published data determine the equation of the straight line v = constant in the tangent plane centred at the reference point.

To minimise the errors due to the projection on the tangent plane, the reference point was chosen in the immediate vicinity of the true, but unknown, position. The reference point has the same abscissa as the observed abscissa of the planet, $v^{\rm obs}$, and a calculated ordinate $r^{\rm calc}$ based on the ephemeris at the reference time. The astrometric position expressed in the reference great-circle frame (RGC) and in the provisional reference frame of the Hipparcos reductions (P, representing either H37C or F37.3) are related by the transformation:

$$\mathbf{u}_{\rm P} = \mathbf{R}_3(\Omega)\mathbf{R}_1(i)\mathbf{u}_{\rm RGC} \qquad [15.17]$$

where i and Ω are the inclination and the longitude of the node of the reference great circle, $\mathbf{R}_k$ represents a rotation about the kth axis, and:

$$\mathbf{u}_{\rm RGC} = \begin{pmatrix} \cos r^{\rm calc} \cos v^{\rm obs} \\ \cos r^{\rm calc} \sin v^{\rm obs} \\ \sin r^{\rm calc} \end{pmatrix}, \qquad \mathbf{u}_{\rm P} = \begin{pmatrix} \cos\delta_0 \cos\alpha_0 \\ \cos\delta_0 \sin\alpha_0 \\ \sin\delta_0 \end{pmatrix} \qquad [15.18]$$

The direction defined in the reference great-circle frame by $v = v^{\rm obs}$ (= constant) is given on the tangent plane, in an indirect manner, by $\theta \in [0, 2\pi[$, the position angle of the reference great circle at the reference point. This angle, reckoned counter-clockwise on the sky from $+\delta$, was computed as the direction of the reference great circle at the point $(v, r) = (v^{\rm obs}, 0)$ and is given by:

$$\cos\theta = \frac{\sin i \, \cos v}{\left(1 - \sin^2 i \, \sin^2 v\right)^{1/2}}, \qquad \sin\theta = \frac{\cos i}{\left(1 - \sin^2 i \, \sin^2 v\right)^{1/2}} \qquad [15.19]$$

The standard error refers to the uncertainty of the abscissa in the direction **w** parallel to the reference great circle and passing through the reference point:

$$\sigma_{v*} = \sigma_v \cos r^{\rm calc} \qquad [15.20]$$

Transformation to International Celestial Reference System

The positions obtained so far are still referred to arbitrary intermediate frames resulting from the Hipparcos sphere solutions (i.e. F37.3 for FAST and H37C for NDAC; see

Table 15.1. Values of the rotation and spin components for the reference frames transformations. The components of the orientation refer to the epoch T_0 = J1991.25.

	Orientation (mas)			Spin (mas/yr)		
	ε_{0x}	ε_{0y}	ε_{0z}	ω_x	ω_y	ω_z
N37.5→H37C	−20.648	−33.151	+46.719	−0.584	+0.657	+0.508
H37C→ICRS	−19.1	−8.5	+20.9	−0.73	+0.05	+0.47
F37.3→ICRS	−24.218	−27.532	+56.190	−0.590	−0.453	+3.661

Chapter 16). The published solar system data must, however, use the same reference system as the stars, namely the International Celestial Reference System, ICRS (Chapter 18). The orientation of P (F37.3 or H37C) with respect to ICRS is given by a time dependent, small rotation $\boldsymbol{\varepsilon}(t) = \boldsymbol{\varepsilon}_0 + (t - T_0)\boldsymbol{\omega}$, where T_0 = J1991.25 is the epoch of the Hipparcos Catalogue. Thus, the final coordinates $\mathbf{u}_{\mathrm{ICRS}}$, referred to the ICRS, were obtained by:

$$\mathbf{u}_{\mathrm{ICRS}} = \begin{pmatrix} 1 & \varepsilon_z & -\varepsilon_y \\ -\varepsilon_z & 1 & \varepsilon_x \\ \varepsilon_y & -\varepsilon_x & 1 \end{pmatrix} \mathbf{u}_{\mathrm{P}} \qquad [15.21]$$

where ε_x, ε_y, ε_z are the equatorial components of $\boldsymbol{\varepsilon}(t)$ for the epoch of the observation. In principle, the transformation entails also a change of the position angle θ, but this change would always be less than 0.1 arcsec and was therefore not implemented. The values of the rotation parameters for the transformations H37C→ICRS and F37.3→ICRS are listed in Table 15.1.

Comparison of FAST and NDAC Abscissae

The methods applied by FAST and NDAC to process the observations of the solar system objects were generally very similar. However they differed sufficiently in their details to prohibit a merging of the two sets of abscissae.

The positions on the grid were not derived in the same way from the signal phases which implies that the observed positions do not correspond to exactly the same physical point. This discrepancy depends mainly on the object's size, and to a lesser extent on its shape, on its brightness distribution, and on the geometry of the scanning direction relative to the visible surface. The theoretical differences between the Hipparcos position and the photocentre were shown in Figure 15.1 for a spherical object of uniform brightness, and although they are not large, they are not identical for FAST and NDAC.

The systematic phase effect was shown by Söderhjelm & Lindegren (1982) to have a non-negligible influence on the realisation of the dynamical reference frame from the Hipparcos observations of solar system objects. As noted previously, these effects cannot be predicted with sufficient accuracy to be accounted for and could have different consequences in the FAST and NDAC treatments.

For all these reasons, and in order to avoid introducing additional noise in the data, it was thought preferable to publish separately the FAST and NDAC results for all the

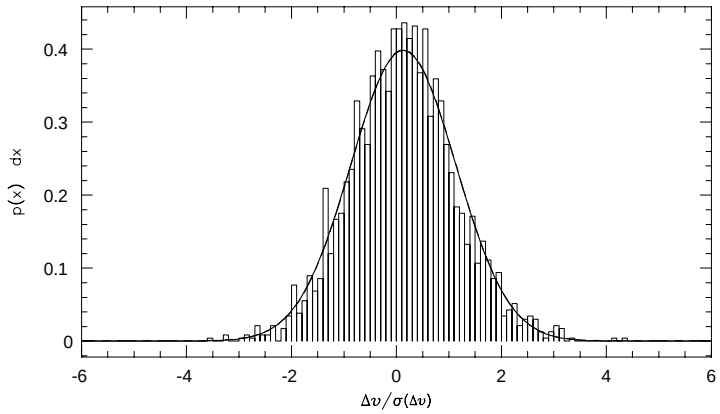

Figure 15.7. *Comparison of FAST and NDAC abscissae from the reference points in the ICRS. The histogram represents the normalised difference with a correlation factor of 0.85 (determined from faint stars) and weighted standard deviations. The solid curve is the corresponding Gaussian of unit variance* $\Delta v/\sigma_{\Delta v} \in N(0.13, 1)$*, the non-normalised mean offset is* $\langle \Delta v \rangle \simeq 1.2$ *mas.*

solar system objects. However, from the calibration of the FAST and NDAC procedures with respect to the stars, it is expected that:

$$\lim_{\rho \to 0} v_{\mathrm{NDAC}} \simeq \lim_{\rho \to 0} v_{\mathrm{FAST}} \simeq v_{\mathrm{photocentre}}$$

which means that the FAST and NDAC abscissae should be very similar for the smallest planets ($\rho \ll s$). Figure 15.7 shows an histogram of the normalised differences between the FAST and NDAC abscissae. The average of the normalised differences is slightly positive, corresponding to a systematic difference between the FAST and NDAC abscissae of about 1.2 mas. However, the abscissae are not strictly referred to the same circles since they have been defined independently by each group. The projections of the planets may thus be marginally different.

Finally, for objects as large as $\simeq 0.7$ arcsec, depending on their actual brightness distribution, the second harmonic vanishes (see Equation 15.9 and Figure 15.2) and the corresponding phase ψ of Equation 15.2 becomes meaningless. A consequence of this was that only NDAC positions could be derived for the planetary satellites J2 Europa and S6 Titan.

15.5. Photometry of the Solar System Objects

FAST Reduction

The photometric reduction of the solar system objects was done only by the FAST Consortium, in parallel with that of the stars. The apparent magnitudes in the Hp scale are provided at a rate of one value for every field transit in exactly the same way as for the stars and in the same photometric system, using the colour $B - V = 0.5$ mag for all the planets (see Chapter 14).

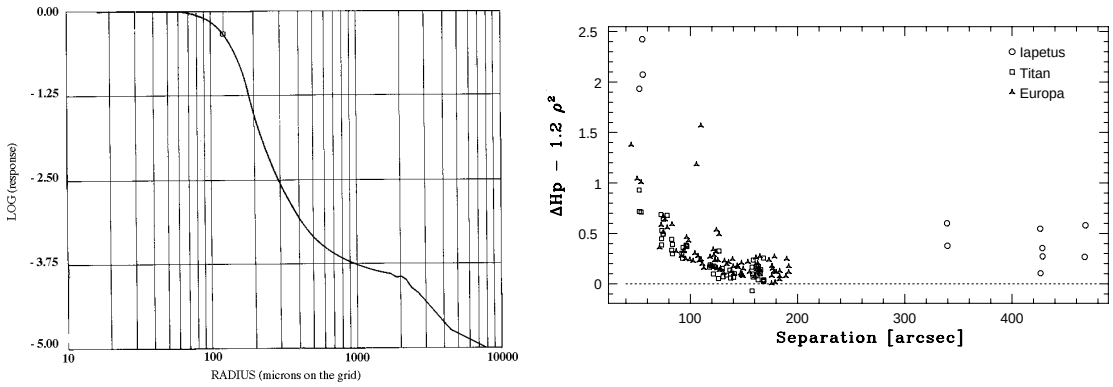

Figure 15.8. *Attenuation profile of the instantaneous field of view. Left: average profile from on ground calibration (1 μm $\simeq$ 0.147 arcsec). The actual in-flight profile is unknown between 100 and 500 arcsec. Right: magnitude difference ΔHp corrected for bias due to the modulation, as a function of the angular separation between the planet (Jupiter or Saturn) and its observed satellite.*

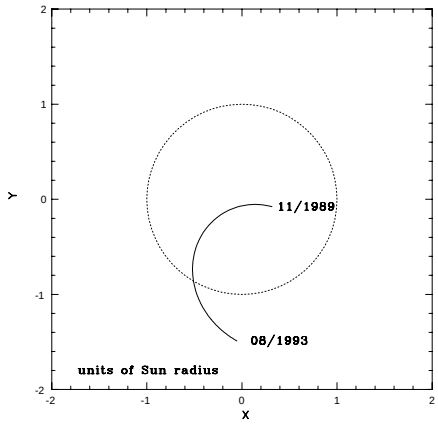

Figure 15.9. *Position of the solar system barycentre during the mission (solid line). Rectangular coordinates of the barycentre in the ecliptic plane.*

However, for the three planetary satellites on the programme, diffusion of the light of their respective planets considerably perturbed the observations and no satisfactory solution could be reached. The average instantaneous field of view profile is given for large offsets in Figure 15.8. With a planet 7 or 8 mag brighter than the satellite and located only a few hundreds of seconds off the centre of the field of view, there is still some planetary light perturbing the signal of the satellite. The effect is hard to assess because the exact attenuation profile is not known in the periphery of the instantaneous field of view. Figure 15.8 (right) shows the difference between the two magnitudes scales $Hp_{\rm ac}$ and $Hp_{\rm dc}$ after the expected effect due to the apparent size of a satellite has been removed. The remaining differences, which should be zero, were sampled as a function of the separation between the satellite and the planet at the time of observation. This unmodelled difference reflects essentially the residual disturbing light originating from the planet. The consequence on the photometric measurement is fairly large for any satellite whatever the separation to such an extent that no reliable magnitude could be provided.

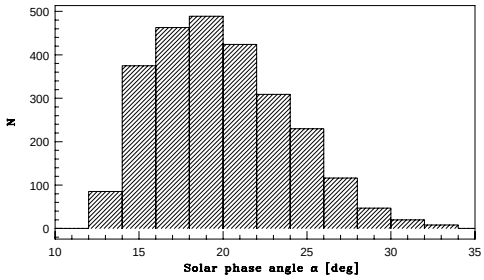

Figure 15.10. *Distribution of the solar phase angle of the minor planets during the Hipparcos mission. The scanning law imposed that the observations could only occur in the vicinity of the quadratures, in contrast with the prevailing situation for ground-based observations.*

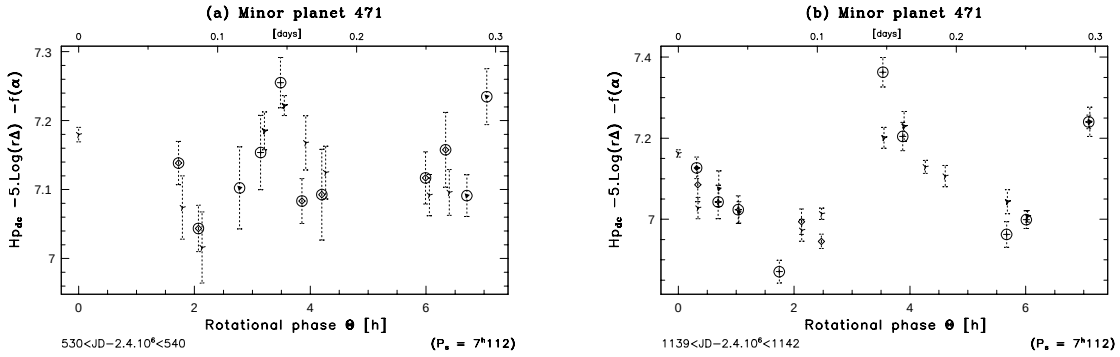

Figure 15.11. *Folded light curves for (471) Papagena obtained at different epochs. The magnitudes are corrected for the distance to the Earth (Δ) and the Sun (r), and for solar phase angle (α). (a) epoch $t \simeq 530$, the circled points correspond to observations made about 10 days later; (b) epoch $t \simeq 1140$, the circled points correspond to observations made about 3 days later.*

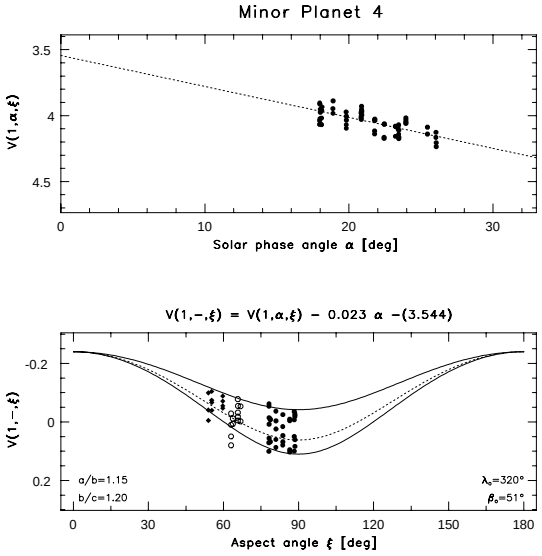

Figure 15.12. *Magnitude-phase (top) and magnitude-aspect (bottom) relations for minor planet (4) Vesta. The solid curves in the magnitude-aspect plot correspond to a triaxial ellipsoid model ($a : b : c = 1.15 : 1.2 : 1$), the dotted curve corresponds to the synthesis model of ratio ($a : b : c = 1.1 : 1.2 : 1$) from Magnusson et al. (1994).*

To help interpret the apparent magnitudes of the minor planets, the geometric parameters at the time of observations are also provided with the solutions. This includes the distance to the solar system barycentre, the distance to the Earth, the phase angle (the angle between the satellite and the Sun as seen from the minor planet's centre of mass) and the apparent diameter, based on the IRAS Catalogue (Tedesco 1989).

The observed apparent magnitudes of minor planets being accurate to a few hundredths of a magnitude, the geocentric distance of the Hipparcos satellite can be neglected. As for the Sun, over the observation period, the solar system barycentre was always within 1.6 solar radii of the centre of the Sun, so that the offset distance barycentre-centre of the Sun may also be disregarded (see Figure 15.9).

The estimator $Hp_{\rm ac}$ is also provided for the sake of completeness, although it is not very useful for planets of large diameter. Transits rejected during the astrometric reduction are also discarded for the photometric output. All magnitudes are given in the *Hp* system and can be transformed to standard V magnitudes with the expressions given in Tables 14.1 and 14.2.

Minor Planet Brightness Variations

Due to the scanning law of the satellite, the observations of minor planets took place when the planets were close to their quadratures and were not uniformly distributed over the rotational phases of the planets. The distribution of the phase angles is shown in Figure 15.10 for all the observations of the minor planets. The mean value of the order of 20° is a consequence of the observations having been made near quadrature.

Table 15.2, based on the Asteroids II data base (Magnusson 1989) and its updated version (Magnusson *et al.* 1994), indicates what is known about the shapes and poles of the minor planets, information relevant for the interpretation of the Hipparcos epoch photometry of the minor planets. Summary statistics related to the conditions of observations of the 48 minor planets are listed in Table 15.3.

An example of a photometric analysis is shown in Figure 15.11 with the folded light curves of (471) Papagena. The curves were computed with a rotation period of 7.11 hr and the magnitudes are absolute, i.e. corrected for the varying distances from the Sun and the Earth. A correction was also applied for the phase angle to show the variation with aspect. The variation with the solar phase angle and the aspect angle is illustrated for (4) Vesta in Figure 15.12. The amplitude of the magnitude-aspect relation is smaller for objects observed at opposition.

D. Hestroffer, F. Mignard

Table 15.2. Tholen's taxonomic classification (Tholen 1989) for Hipparcos minor planets. Poles and shapes (as by-products of pole determinations) solution, from Asteroids II (Magnusson 1989) and updated version (Magnusson *et al.* 1994).

IAU Number and Name	Tholen class	Asteroids II data base	Solution pole	Solution shape	Updated version	Solution pole	Solution shape
(1) Ceres	G	√	√	√	√	√	√
(2) Pallas	B	√	√	√	√	√	√
(3) Juno	S	√	√	√	√	√	√
(4) Vesta	V	√	√	√	√	√	√
(5) Astraea	S	√	√	√	√	√	√
(6) Hebe	S	√	√	√	√	√	√
(7) Iris	S	√	√	√	√	√	√
(8) Flora	S	√	√	–	√	√	√
(9) Metis	S	√	√	√	√	√	√
(10) Hygiea	C	√	–	–	√	√	√
(11) Parthenope	S	–	–	–	–	–	–
(12) Victoria	S	√	√	–	√	√	√
(13) Egeria	G	–	–	–	–	–	–
(14) Irene	S	–	–	–	–	–	–
(15) Eunomia	S	√	√	√	√	√	√
(16) Psyche	M	√	√	√	√	√	√
(18) Melpomene	S	–	–	–	√	√	–
(19) Fortuna	G	√	√	√	√	√	√
(20) Massalia	S	√	√	√	√	√	√
(22) Kalliope	M	√	√	√	√	√	√
(23) Thalia	S	–	–	–	√	√	√
(27) Euterpe	S	–	–	–	–	–	–
(28) Bellona	S	√	√	√	√	√	√
(29) Amphitrite	S	√	√	√	√	√	√
(30) Urania	S	–	–	–	–	–	–
(31) Euphrosyne	C	√	√	√	√	√	√
(37) Fides	S	√	√	√	√	√	√
(39) Laetitia	S	√	√	√	√	√	√
(40) Harmonia	S	–	–	–	√	√	√
(42) Isis	S	–	–	–	–	–	–
(44) Nysa	E	√	√	√	√	√	√
(51) Nemausa	CU	–	–	–	√	√	√
(63) Ausonia	S	√	√	√	√	√	√
(88) Thisbe	CF	√	√	√	√	√	√
(115) Thyra	S	–	–	–	√	√	√
(129) Antigone	M	√	√	√	√	√	√
(192) Nausikaa	S	√	√	–	√	√	√
(196) Philomela	S	–	–	–	√	√	√
(216) Kleopatra	M	√	√	√	√	√	√
(230) Athamantis	S	–	–	–	–	–	–
(324) Bamberga	CP	–	–	–	–	–	–
(349) Dembowska	R	√	√	√	√	√	√
(354) Eleonora	S	√	√	√	√	√	√
(451) Patientia	CU	√	√	√	√	√	√
(471) Papagena	S	–	–	–	–	–	–
(511) Davida	C	√	√	√	√	√	√
(532) Herculina	S	√	√	√	√	√	√
(704) Interamnia	F	√	√	–	√	√	√

Table 15.3. Hipparcos minor planets general statistics on aspect data. Minimum (min), maximum (max) and median (med) value for the observation epoch, and the apparent magnitude $Hp_{\rm dc}$.

Num (IAU)	Obs	Epoch (JD-2440000.0 [day])			Magnitude ($Hp_{\rm dc}$)			Standard deviation ($\sigma_{Hp_{\rm dc}}$)		
		min	med	max	min	med	max	min	med	max
1	65	7920.570	8522.710	8977.859	7.84	9.20	9.49	0.004	0.009	0.024
2	63	8154.100	8728.980	8934.850	8.51	9.57	10.78	0.003	0.014	0.053
3	60	7909.230	8391.870	9038.870	8.42	10.60	11.55	0.003	0.018	0.036
4	58	8084.980	8351.210	8817.159	7.15	8.26	8.69	0.002	0.006	0.019
5	81	8094.660	8393.780	8832.319	10.23	11.50	12.36	0.005	0.029	0.077
6	91	7870.420	8082.890	8967.080	8.67	10.55	11.67	0.001	0.016	0.048
7	69	7911.560	8560.680	9024.380	8.24	9.83	11.31	0.001	0.013	0.040
8	56	7917.310	8503.030	9035.370	9.94	10.95	11.93	0.006	0.022	0.051
9	40	8142.720	8327.859	8826.890	9.75	10.84	11.90	0.005	0.019	0.033
10	51	8023.670	8479.570	9059.700	10.97	11.57	12.21	0.006	0.026	0.077
11	68	8144.420	8315.500	8823.000	10.71	11.14	12.47	0.006	0.023	0.082
12	24	7880.400	8771.590	8820.340	10.68	11.42	12.33	0.006	0.022	0.055
13	34	8053.010	8506.390	8739.971	11.03	11.95	12.38	0.011	0.032	0.074
14	45	7885.640	8540.890	8795.330	10.08	11.47	12.53	0.006	0.023	0.074
15	83	7882.620	8694.800	9044.960	9.51	10.58	11.60	0.004	0.022	0.067
16	49	7894.530	8559.819	9033.670	10.22	11.59	12.56	0.004	0.034	0.076
18	100	7900.880	8354.020	9059.710	10.08	11.36	12.26	0.006	0.028	0.069
19	30	8087.990	8331.940	8787.159	11.15	12.05	12.78	0.014	0.038	0.092
20	61	7984.580	8538.230	8809.290	8.37	11.32	12.29	0.007	0.026	0.058
22	63	8022.960	8675.730	9009.119	10.76	11.92	12.73	0.009	0.034	0.115
23	66	7876.620	8402.000	9022.460	11.02	12.34	12.83	0.009	0.039	0.098
27	35	7884.310	8240.649	8830.990	10.04	11.41	12.20	0.009	0.022	0.064
28	33	8513.319	8961.450	9009.640	11.81	12.14	12.63	0.011	0.043	0.082
29	74	7986.090	8535.090	9006.689	9.86	10.71	11.44	0.003	0.019	0.069
30	48	7860.230	8289.060	8752.380	10.49	12.03	12.84	0.011	0.039	0.179
31	14	7919.690	7966.870	8298.210	11.06	11.82	12.27	0.021	0.030	0.042
37	32	7883.730	7984.820	8935.730	11.25	11.66	13.01	0.009	0.030	0.079
39	112	7858.510	8396.220	8824.830	10.49	11.29	12.57	0.007	0.021	0.059
40	103	7969.470	8708.609	8805.640	10.68	12.20	12.63	0.009	0.039	0.111
42	51	7973.480	8120.000	8278.280	10.26	11.00	12.48	0.007	0.022	0.067
44	53	8021.540	8586.140	8808.840	9.97	11.52	12.35	0.007	0.029	0.052
51	14	8050.070	8067.220	9033.500	11.64	11.79	12.24	0.010	0.032	0.050
63	12	8279.390	8422.020	8945.390	11.51	11.95	12.50	0.010	0.026	0.057
88	36	7960.780	8169.350	8618.330	11.26	12.06	12.51	0.021	0.041	0.063
115	33	7915.230	8758.230	8973.250	10.98	12.38	12.65	0.011	0.042	0.102
129	40	7899.460	8325.319	8563.950	11.51	12.05	12.55	0.015	0.032	0.062
192	32	7916.310	8739.649	8833.640	10.90	11.12	12.15	0.013	0.034	0.074
196	14	7992.570	8139.310	8594.159	11.58	11.93	12.55	0.019	0.037	0.051
216	21	7895.420	8311.500	8359.040	11.37	11.87	12.80	0.008	0.037	0.061
230	35	7908.390	8287.020	8935.980	11.34	11.72	12.44	0.006	0.028	0.066
324	73	8320.710	8325.240	8682.310	9.35	12.11	12.39	0.006	0.028	0.068
349	92	7910.830	8176.370	8634.590	10.28	11.77	12.19	0.009	0.025	0.080
354	98	7899.520	8404.700	9053.119	10.76	11.59	12.55	0.012	0.030	0.088
451	29	8258.271	8632.050	8731.630	11.52	11.91	12.46	0.016	0.033	0.070
471	112	8020.210	8487.649	9024.800	10.84	11.38	12.85	0.005	0.032	0.090
511	64	8046.070	8588.790	9030.040	11.18	12.01	12.66	0.007	0.034	0.107
532	40	7937.440	8398.210	8829.300	10.16	10.91	12.29	0.003	0.021	0.064
704	82	8021.100	8534.090	8735.530	11.07	11.76	12.58	0.008	0.032	0.082

Table 15.3. Hipparcos minor planets general statistics on aspect data (continued). The distances to the Sun and to the Earth, the solar phase angle, and the apparent diameter.

Num (IAU)	Distances (Sun [AU])		Distances (Earth [AU])		Solar phase angle (α [deg])			Apparent diameter (ρ [arcsec])		
	min	max	min	max	min	med	max	min	med	max
1	2.582	2.979	1.864	3.554	14.19	16.09	22.41	0.35	0.40	0.67
2	2.123	3.382	1.733	3.842	13.53	17.43	27.37	0.19	0.29	0.41
3	2.013	3.356	1.309	3.693	14.20	16.65	26.21	0.09	0.12	0.26
4	2.205	2.576	1.712	3.052	17.96	21.77	26.06	0.23	0.28	0.40
5	2.080	2.842	1.369	3.008	15.80	18.02	28.73	0.06	0.08	0.13
6	1.940	2.911	1.207	3.370	14.94	18.99	30.65	0.08	0.13	0.22
7	1.844	2.932	1.131	3.133	16.56	23.29	31.67	0.09	0.12	0.25
8	1.901	2.539	1.447	3.042	17.22	22.72	29.92	0.06	0.08	0.13
9	2.096	2.674	1.371	2.819	19.56	21.35	28.10	0.08	0.12	0.17
10	3.068	3.516	2.564	3.947	13.54	16.08	19.05	0.15	0.18	0.23
11	2.383	2.695	1.815	3.156	15.78	17.78	24.92	0.07	0.11	0.12
12	2.076	2.843	1.421	2.282	16.29	25.16	29.24	0.07	0.09	0.11
13	2.354	2.794	1.755	2.679	18.48	21.63	24.63	0.11	0.13	0.17
14	2.155	3.006	1.454	3.552	14.04	22.34	27.89	0.06	0.09	0.15
15	2.174	3.130	1.865	3.555	13.59	15.12	25.89	0.11	0.16	0.20
16	2.552	3.297	1.901	3.713	14.16	16.77	22.97	0.10	0.12	0.19
18	1.847	2.785	1.495	3.301	15.23	20.64	27.32	0.06	0.08	0.14
19	2.057	2.826	1.711	2.500	16.39	23.22	28.47	0.12	0.15	0.18
20	2.066	2.738	1.555	3.141	17.96	23.02	28.59	0.07	0.08	0.13
22	2.632	3.003	2.071	3.285	15.90	17.76	22.54	0.05	0.06	0.08
23	2.060	3.210	1.641	3.195	13.72	17.79	28.37	0.05	0.06	0.09
27	1.948	2.746	1.225	2.841	17.05	27.21	29.42	0.05	0.07	0.11
28	2.402	2.727	1.932	2.498	19.85	23.21	24.07	0.07	0.08	0.09
29	2.374	2.674	1.648	2.998	17.22	21.82	24.94	0.10	0.14	0.18
30	2.065	2.617	1.344	2.419	16.44	17.87	28.29	0.06	0.08	0.11
31	2.427	3.043	1.786	2.607	17.53	22.61	24.00	0.13	0.15	0.19
37	2.345	3.063	1.592	2.506	14.23	19.33	22.83	0.06	0.08	0.10
39	2.455	3.085	1.912	3.522	13.62	17.64	23.56	0.06	0.09	0.11
40	2.163	2.366	1.445	2.945	18.14	21.83	26.98	0.05	0.06	0.11
42	1.890	2.258	1.110	2.409	20.67	23.54	32.30	0.06	0.11	0.13
44	2.073	2.769	1.375	2.776	20.51	23.48	28.34	0.04	0.04	0.07
51	2.222	2.458	1.688	1.934	19.98	21.23	26.37	0.11	0.12	0.12
63	2.205	2.455	1.689	2.163	19.53	23.52	26.52	0.07	0.08	0.09
88	2.346	2.720	1.704	2.730	17.59	21.58	23.75	0.11	0.14	0.17
115	2.007	2.567	1.339	2.572	21.32	23.01	28.35	0.04	0.05	0.09
129	2.287	2.778	2.052	2.800	18.21	20.86	24.91	0.06	0.07	0.08
192	2.144	2.546	1.435	2.083	18.89	19.67	25.90	0.07	0.10	0.10
196	3.029	3.103	2.399	2.948	16.59	18.63	19.24	0.07	0.08	0.08
216	2.230	2.727	1.861	2.763	17.14	19.74	25.94	0.07	0.09	0.10
230	2.272	2.523	1.718	2.494	16.68	18.46	25.26	0.06	0.09	0.09
324	1.771	2.401	0.936	2.970	17.46	18.32	32.60	0.11	0.11	0.36
349	2.678	3.174	2.107	3.620	13.89	14.40	21.29	0.05	0.05	0.09
354	2.479	3.001	1.946	3.593	13.84	18.26	23.16	0.06	0.07	0.11
451	2.845	3.040	2.119	2.719	14.35	17.69	20.29	0.12	0.14	0.15
471	2.279	3.349	1.695	3.155	14.87	17.49	25.28	0.06	0.10	0.11
511	2.631	3.351	2.207	3.562	14.61	18.48	22.05	0.13	0.16	0.21
532	2.329	3.135	1.906	3.654	14.22	20.32	24.74	0.09	0.13	0.17
704	2.614	3.118	2.137	3.364	14.05	18.02	22.04	0.14	0.16	0.21